Non-equilibrium Evolution of Water Resources and Future Trend Projections in the Xiabuqu River Basin

Siyu Lai[1, 2], Baodeng Hou[2, *] and Nanjia Zaxi[3]

[1]Key Laboratory of Regional Energy and Environmental Systems Optimization, Ministry of Education, North China Electric Power University, Beijing 102206, China

[2]State Key Laboratory of Water Cycle and Water Security, China Institute of Water Resources and Hydropower Research, Beijing 100038, China

[3]Xizang Bainang County Water Conservancy Team, Shigatse 857300, China

[*] Corresponding author

Abstract

Runoff in the Xiabuqu River Basin, a first-order tributary of the Yarlung Zangbo River, was reconstructed by combining WEP-L with HMETS and a degree-day glacier-melt module. The coupled scheme yielded an NSE of 0.8158, higher than the performance of the individual runoff models. For 1978–2020, the reconstructed annual water-resource volume averaged 754 million m^3, but varied considerably from year to year. Rainfall supplied 94.69% of runoff on average, whereas snowmelt and glacier melt made much smaller contributions. Projections under SSP245 and SSP585 indicate a modest decrease in mean water resources over the next three decades. Meanwhile, interannual and seasonal variability increases, suggesting less stable water availability and a greater likelihood of both wet and dry extremes.

Keywords

Runoff simulation; hydrological model; climate model; trend projection; Qinghai–Tibetan Plateau; Xiabuqu River.

1. INTRODUCTION

The Xiabuqu River is a first-order tributary of the Yarlung Zangbo River in Shigatse, Tibet Autonomous Region. Its catchment covers about 5,417 km^2 and lies mostly above 4,000 m. Runoff is generated not only by rainfall but also by seasonal snow and glacier melt, so annual water availability is sensitive to both precipitation variability and temperature-related changes in snow and ice. This combination of a high-elevation setting and multiple runoff sources makes the basin a useful case for examining how alpine water resources respond to a changing climate.

Previous hydrological studies of small cold-region basins on the plateau have often treated individual runoff processes separately, and long-term assessments that combine rainfall, snowmelt, glacier melt, and future climate forcing are still relatively limited. We therefore organized the analysis in three steps. First, alternative runoff simulations were compared and coupled to obtain a basin-scale runoff series. The calibrated model was then used to reconstruct historical water-resource changes and separate the main runoff components. Finally, the same framework was driven by climate-model data to examine possible changes in future water availability.

ISSN: 2472-3703 DOI: 10.6911/WSRJ.202609_12(9).0012

2. METHODS

2.1. Study Area

The Xiabuqu River Basin extends from 88°06′ to 89°17′ E and from 28°17′ to 29°18′ N. The main river is about 185 km long, and most of the basin lies within Bainang and Sakya counties. Terrain generally rises toward the watershed divide, where elevations are commonly above 4,800 m; the highest point reaches 6,092 m. The basin has a plateau temperate semi-arid monsoon climate. Long-term mean air temperature is 4.8 °C, annual precipitation is about 327 mm, mean relative humidity is 43%, and annual sunshine duration is approximately 3,200 h. Vegetation cover is sparse. Cropland is concentrated mainly along the reaches from Saixiang to Laluo and from Kudui to the basin outlet. River flow is supplied by rainfall, snow-and-ice melt, and groundwater, and the upper reaches usually freeze in winter.

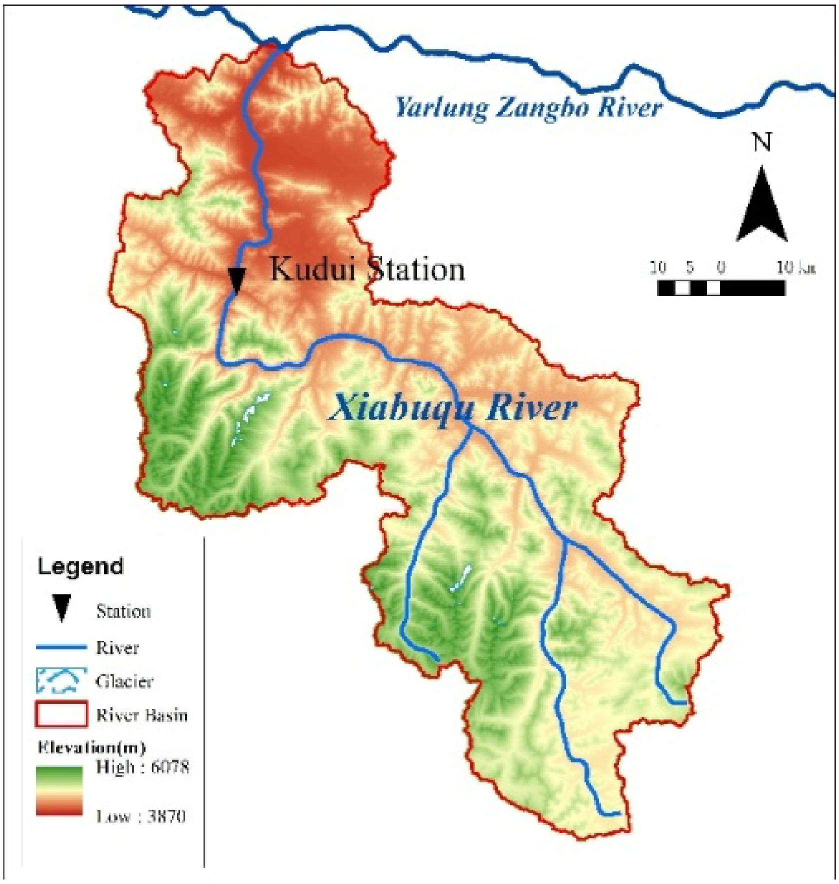

Figure 1. Overview of the Xiabuqu River Basin

2.2. Development of the Runoff Prediction Model

Runoff in the Xiabuqu River Basin has several sources, so the rainfall-runoff and snow-and-ice-melt components were represented separately before being combined. WEP-L [1] and the Xinanjiang model [2] were each used to simulate rainfall-runoff generation and routing. Snowmelt and glacier-melt contributions were estimated with HMETS [4] and the degree-day factor method [3], respectively. The resulting runoff components were then combined and evaluated against observations, and the model combination with the best overall performance was retained for the subsequent analyses.

ISSN: 2472-3703 DOI: 10.6911/WSRJ.202609_12(9).0012

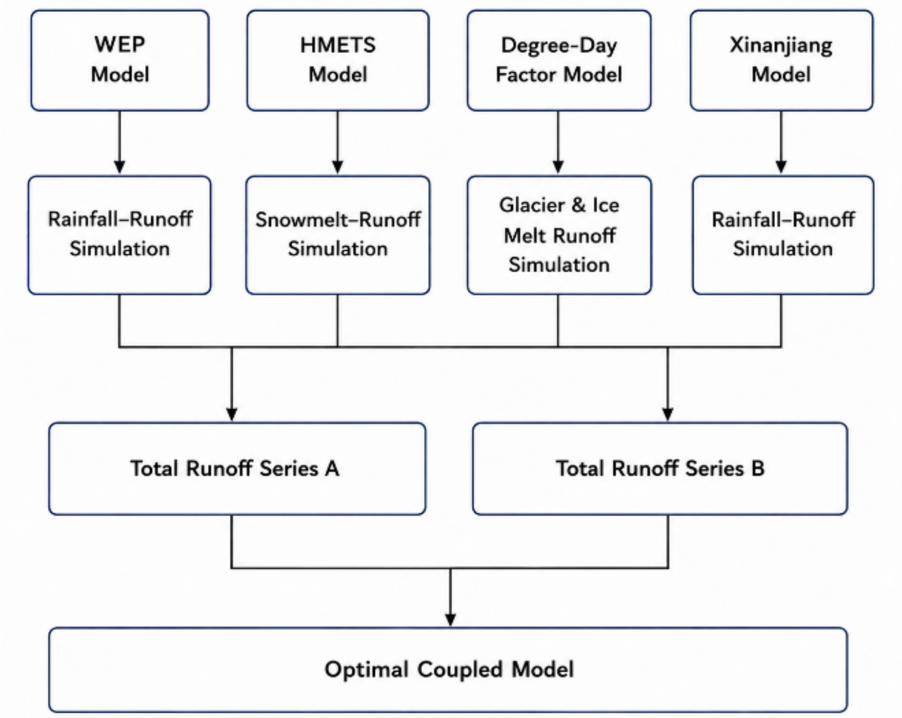

Figure 2. Configuration of the runoff-simulation and model-coupling procedure

For WEP-L, the basin was discretized by sub-basin and elevation band following the method described in [5]. The river network was extracted from the DEM and used to define the computational units [6]. Meteorological forcing for 1977–2020 was supplied together with period-specific land-use data. The positions of key hydrological nodes, including the Kudui Hydrological Station, were checked and corrected before the simulation was run.

The Xinanjiang model was configured with its conventional three-source runoff structure. Evapotranspiration, runoff generation, runoff partitioning, and routing were calculated successively. To examine the influence of meteorological forcing, three input-data schemes were tested. Initial parameter ranges were set with reference to previous applications in basins with similar hydrological conditions.

Glacier melt was calculated with the degree-day method using glacier distribution, temperature, and the corresponding degree-day factors. Seasonal snowmelt was treated separately with the HMETS snow module, for which MODIS snow-cover information was used as an additional constraint. The two simulated components were subsequently added to the rainfall-runoff results.

2.3. Evaluation of Simulation Performance

The Nash–Sutcliffe efficiency coefficient (NSE) and the square of the Pearson correlation coefficient (R^2), which are commonly used in hydrological simulation, were selected to evaluate model performance:

NSE measures the agreement between simulated and observed runoff. It ranges from (−∞, 1], and NSE ≥ 0.7 was regarded as meeting the required simulation accuracy.

$$NSE = 1 - \frac{\sum_{i=1}^{n}\left(Q_s^i - Q_o^i\right)^2}{\sum_{i=1}^{n}\left(Q_o^i - \bar{Q}_o\right)^2} \tag{1}$$

R^2 was used to describe the linear association between observed and simulated runoff. Values approaching 1 indicate that the two series vary more consistently.

ISSN: 2472-3703 DOI: 10.6911/WSRJ.202609_12(9).0012

$$R^2 = \frac{\left[\sum_{i=1}^{n}\left(Q_s^i - \bar{Q}_s\right)\left(Q_o^i - \bar{Q}_o\right)\right]^2}{\sum_{i=1}^{n}\left(Q_s^i - \bar{Q}_s\right)^2 \sum_{i=1}^{n}\left(Q_o^i - \bar{Q}_o\right)^2} \tag{2}$$

where $Q^o{}_i$ and $Q^s{}_i$ denote the observed and simulated discharge at time i, respectively; $\bar{Q}^o$ and $\bar{Q}^s$ are their corresponding mean values; and n is the number of observations.

The observed and simulated discharge records were first aligned at the monthly scale. NSE and R^2 were then calculated from the paired monthly series and considered together when assessing how well the model reproduced the observed runoff process.

2.4. Data Sources

Model construction required meteorological, topographic, land-surface, hydrological, glacier, and snow-cover datasets. Their temporal ranges and spatial formats differed, so the datasets were processed separately before being introduced into the model. The following subsections describe the source and treatment of each dataset.

(1) Meteorological data

CMFD2.0 was used as the gridded meteorological forcing for 1977–2020. Variables corresponding to the available station observations were extracted over the basin. Before model input, the gridded series were corrected against observations from the three meteorological stations to reduce systematic differences between the two data sources.

Table 1. Basic information on ground meteorological stations

Station ID	Name	Longitude (°)	Latitude (°)	Elevation (m)
55569	Lhatse	87.60	29.08	4000
55578	Shigatse	88.88	29.25	3836
55680	Gyantse	89.60	28.92	4040

The reanalysis dataset is the China Meteorological Forcing Dataset version 2.0 (CMFD2.0), covering 1977–2020 and containing meteorological variables corresponding to the station observations. During preprocessing, the reanalysis data were bias-corrected using ground-station observations to improve their reliability in high-elevation areas.

(2) Topography

Topographic data were obtained from ASTER GDEM V3 at a spatial resolution of 30 m, covering the entire Xiabuqu River Basin. The dataset meets the requirements for river-network extraction, sub-basin delineation, and elevation-band definition. Before use, map-sheet mosaicking, coordinate transformation, and boundary clipping were conducted in ArcMap to produce a seamless elevation dataset for the study area.

(3) Land-surface data

Land-use and soil information was used to characterize the basin surface. Land-use maps were taken from the China Multi-Period Land Use/Cover Remote Sensing Monitoring Dataset provided by the Resource and Environment Science and Data Center of the Chinese Academy of Sciences [7]. Cropland, forest, grassland, built-up land, and their secondary classes were retained, and the land-use map corresponding to each modelling period was used in WEP-L.

(4) Hydrology

Monthly discharge observations at the Kudui Hydrological Station for 2007–2020 were provided by the Hydrology and Water Resources Survey Bureau of the Tibet Autonomous

ISSN: 2472-3703 DOI: 10.6911/WSRJ.202609_12(9).0012

Region. Kudui is the only station within the Xiabuqu River Basin that provides a long and continuous runoff record for the study period. These observations were therefore used as the main reference series for model calibration, validation, and performance assessment.

(5) Glaciers and snow cover

Glacier distribution, degree-day factors, and snow cover were treated as separate cryospheric inputs. Glacier boundaries were taken from the four-period Qinghai–Tibetan Plateau glacier inventory for 1976, 2001, 2013, and 2017 reported by Ye et al. [8]. Degree-day factors were obtained from the High Mountain Asia spatial dataset of Zhang et al. [9]. Snow-covered area was derived from the China MODIS Daily Cloud-Free 500 m Snow-Covered Area Product Dataset (http://www.geodata.cn). For each year, the mean daily snow-covered area from June to September was extracted for the Xiabuqu River Basin and used to characterize summer snow-cover conditions.

(6) Climate models

Future meteorological forcing was taken from the CMIP6-based dataset developed for the Qinghai–Tibetan Plateau by Wang et al. [10]. Daily precipitation and maximum and minimum temperature are available for 1979–2013 and 2015–2100 under SSP126, SSP245, SSP370, and SSP585. The published dataset combines seven CMIP6 models, including ACCESS-ESM1-5. According to Wang et al. [10], ANU-Spline was used for spatial downscaling, Bayesian model averaging for the multi-model ensemble, and CNCDFm for bias correction. The processed series were used directly as future meteorological inputs in this study.

3. RESULTS AND DISCUSSION

3.1. Model Calibration and Validation

In the comparison of runoff-simulation accuracy for the basin upstream of the Kudui Hydrological Station, the WEP model achieved an NSE of approximately 0.72, whereas the Xinanjiang model achieved an NSE of approximately 0.65. New coupled runoff series were generated by adding snowmelt runoff, glacier-melt runoff, and other snow-derived runoff components to the outputs of the two models. The NSE values increased to 0.8158 and 0.7568, respectively; the corresponding R^2 values were 0.8325 and 0.7654; and the mean cumulative relative errors were 0.0421% and 0.0625%. The runoff series produced by coupling the WEP model with the HMETS and degree-day factor models was ultimately selected as the simulation result.

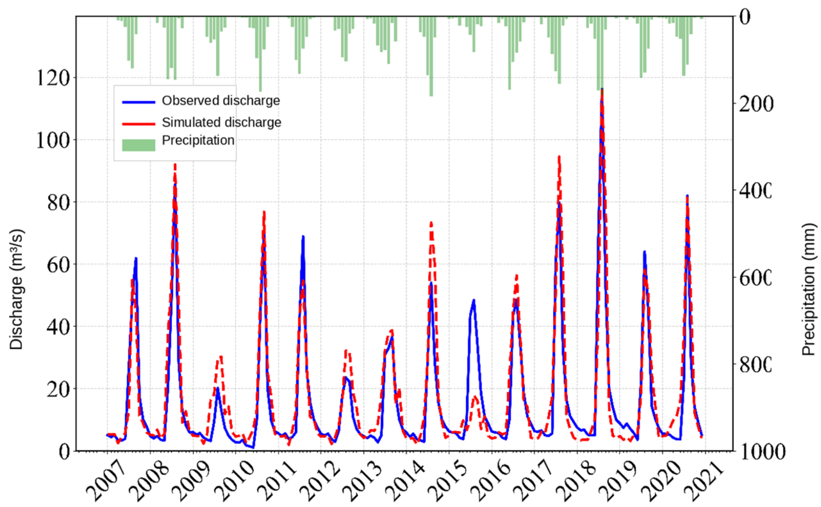

Figure 3. Calibration comparison of discharge at the Kudui Hydrological Station using the coupled model

ISSN: 2472-3703 DOI: 10.6911/WSRJ.202609_12(9).0012

On this basis, the WEP–HMETS–degree-day combination was used in the subsequent reconstruction because it produced the highest NSE and R^2 among the tested schemes.

3.2. Water-Resource Evolution and Driving Mechanisms

As a first-order tributary of the Yarlung Zangbo River, the evolution of water resources in the Xiabuqu River Basin is jointly controlled by climate, topography, and underlying-surface conditions. Historical observations and coupled-model simulations for 1978–2020, runoff-component analysis, and regional hydrological comparisons were combined to identify its evolution patterns and driving mechanisms.

(1) Pronounced interannual fluctuations and a declining decadal tendency in total basin water resources

Across 1978–2020, simulated annual total water resources averaged 754 million m^3, but the series showed large year-to-year differences. The lowest value occurred in 2006, at 241 million m^3, whereas 1978 reached 1.769 billion m^3. The standard deviation over the full period was about 274 million m^3, which is consistent with the strong interannual fluctuations visible in Figure 4.

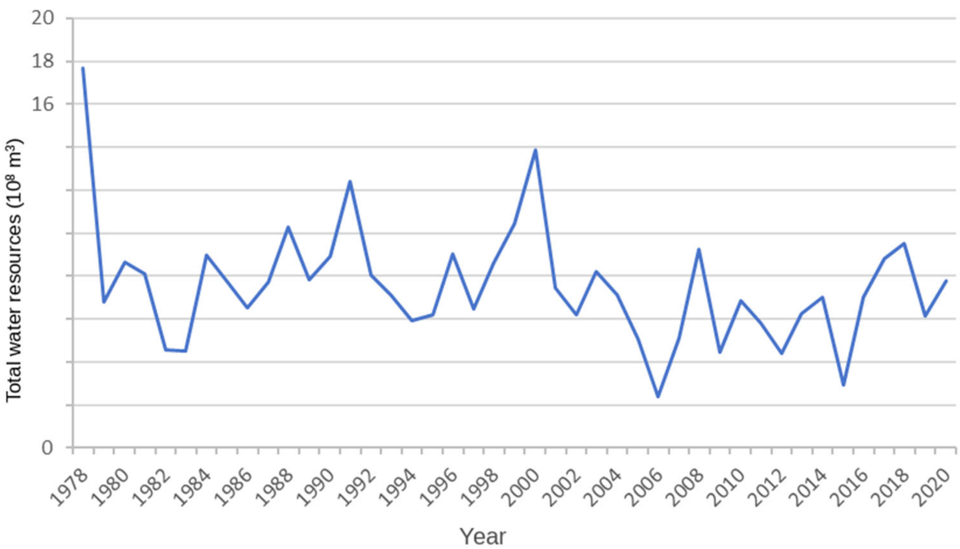

Figure 4. Interannual variation in total water resources in the Xiabuqu River Basin, 1978–2020

(2) Contrast between representative wet and dry years

The contrast between representative wet and dry years is pronounced. Annual water resources reached 1.769 billion m^3 in 1978 and 1.389 billion m^3 in 2000, with most of the water concentrated in the flood season. By comparison, the annual totals fell to 241 million m^3 in 2006 and 295 million m^3 in 2015. From June to September, runoff in those two dry years was only 161 million m^3 and 179 million m^3, respectively, compared with a 1978–2020 mean of 563 million m^3 for the same four-month period.

This contrast points to summer rainfall as the main source of the large differences among years. When summer precipitation is low, the reduction in flood-season runoff is large enough to lower annual water availability markedly, increasing the likelihood of water shortage in dry years.

(3) Contributions of rainfall, snowmelt, and glacier melt

Runoff-component separation at the Kudui Hydrological Station shows a strongly rainfall-dominated regime. Over 1978–2020, rainfall runoff accounted for 94.69% of the annual total

ISSN: 2472-3703 DOI: 10.6911/WSRJ.202609_12(9).0012

on average. Snowmelt contributed 3.90%, and glacier melt contributed 1.41%. The latter two components were therefore small in the annual water balance, but their relative contribution changed between wet and dry years.

The contrast is clear in the two extreme years. In 1978, when annual runoff was the highest in the series, rainfall contributed 95.98%. In 2006, the driest year, the rainfall share fell to 88.47%, while snowmelt increased to 10.21%, well above its long-term average. Snowmelt thus supplied a larger fraction of river flow when rainfall was deficient, although the additional meltwater was far too small to offset the overall reduction in annual runoff.

The component results indicate that year-to-year changes in total water resources largely follow rainfall variability. Snowmelt and glacier melt contribute much less to the annual total, but their relative importance increases when rainfall runoff is low. The 2006 case illustrates this difference: snowmelt accounted for 10.21% of runoff, compared with a long-term mean of only 3.90%.

3.3. Projected Future Changes in Water Reources

Future simulations were compared with the reconstructed 1978–2020 series to examine changes in both total water resources and runoff composition. SSP245 and SSP585 are discussed below as representative medium- and high-emission scenarios.

(1) The simulations indicate a small reduction in mean water resources during the next 30 years. The corresponding averages are 652 million m^3 under SSP245 and 712 million m^3 under SSP585, compared with 754 million m^3 during 1978–2020 (Figures 5 and 6). Thus, neither scenario produces a large change in the long-term mean, although both are lower than the historical value. The simulations also indicate greater water loss under warmer conditions, which partly offsets the projected increase in precipitation.

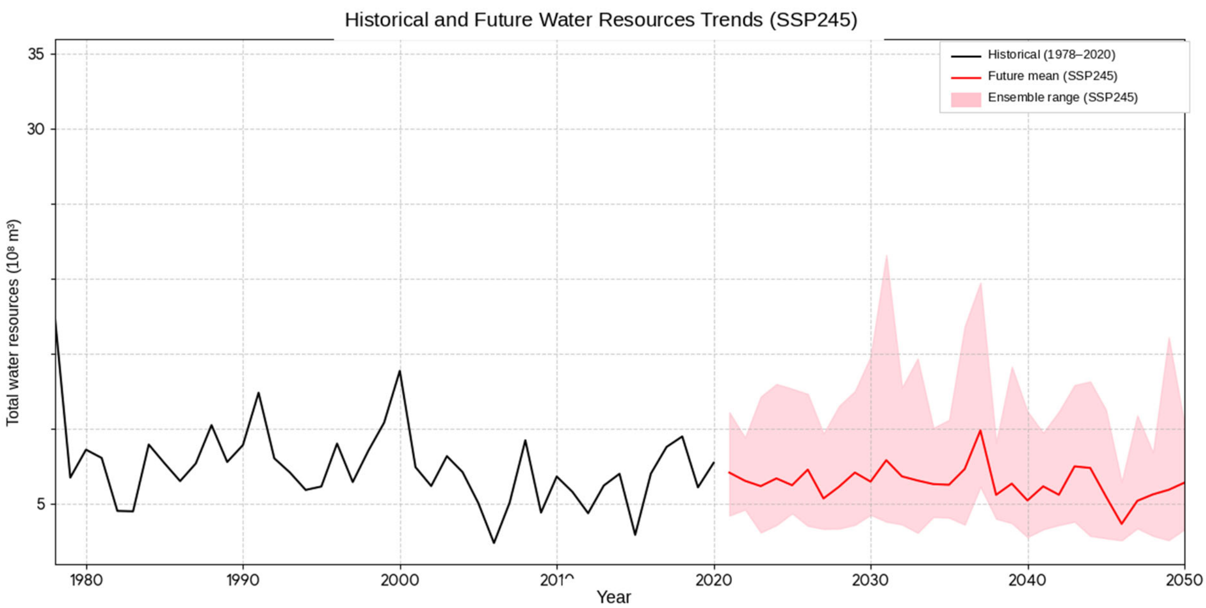

Figure 5. Projected annual total water resources in the Xiabuqu River Basin under SSP245

ISSN: 2472-3703 DOI: 10.6911/WSRJ.202609_12(9).0012

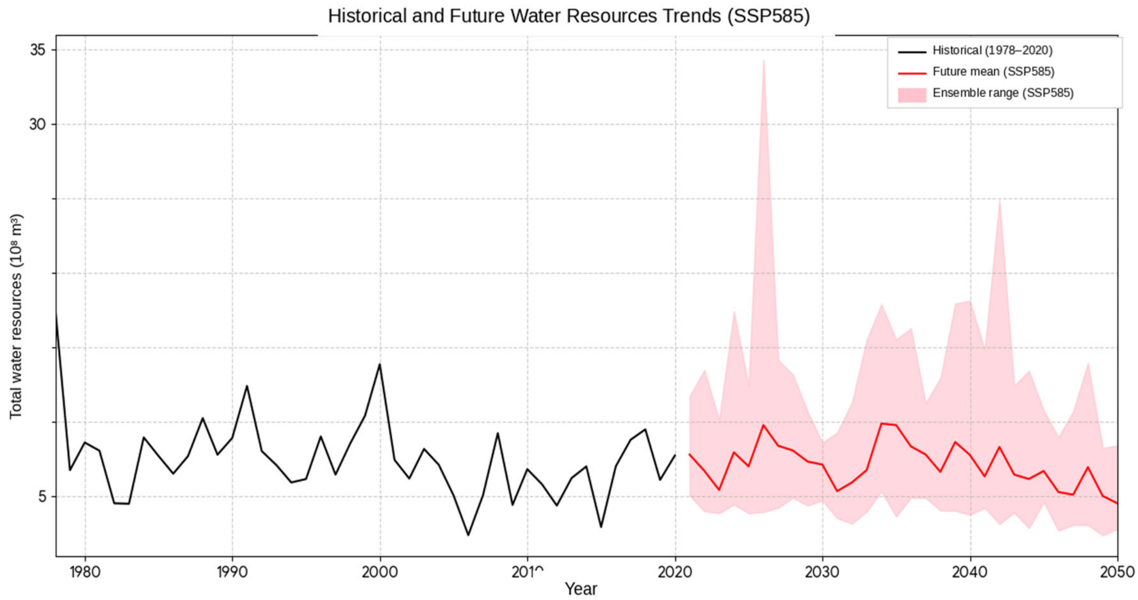

Figure 6. Projected annual total water resources in the Xiabuqu River Basin under SSP585

Changes in variability are more evident than changes in the long-term mean. The future series in Figures 5 and 6 show wider year-to-year fluctuations than the historical reconstruction. At the same time, the projected reduction in glacier and persistent snow contributions weakens the buffering effect provided by solid-water storage. As rainfall and seasonal snowmelt account for most of the runoff, future water availability becomes more dependent on year-to-year meteorological conditions. Consequently, differences between wet and dry years may become larger even though the change in mean annual water resources remains relatively small.

(2) The projected runoff changes can be interpreted in relation to temperature, precipitation, and evapotranspiration changes in the climate forcing.

Rising temperature affects the snow- and glacier-fed components by changing the duration and amount of solid-water storage. In the future simulations, these components decrease and therefore provide a smaller contribution to runoff than during the historical period.

Precipitation changes act differently. Although the projected mean precipitation does not decrease substantially, its temporal variability affects the amount and timing of rainfall-generated runoff. Because rainfall provides most of the basin runoff, these fluctuations are transferred directly to the simulated water-resource series.

A third pathway is enhanced evapotranspiration. Higher temperatures increase atmospheric evaporative demand and can raise both soil evaporation and vegetation transpiration. In the simulations, this additional loss reduces the fraction of precipitation that appears as runoff and contributes to the projected decline in available water resources.

Taken together, these mechanisms do not produce a uniform hydrological response. Changes in snow and glacier storage, precipitation variability, and evapotranspiration act at the same time and sometimes in opposing directions. The projected result is a basin with weaker natural regulation and greater sensitivity to year-to-year climate variability rather than a simple monotonic change in runoff.

ISSN: 2472-3703 DOI: 10.6911/WSRJ.202609_12(9).0012

4. CONCLUSIONS

Three main findings emerge from the historical reconstruction, runoff-component analysis, and future projections:

(1) Coupling WEP with the HMETS and degree-day components improved the runoff simulation at Kudui Station. NSE increased from 0.72 for WEP alone to 0.8158 for the selected coupled scheme, with a mean cumulative relative error of 0.0421%.

(2) Reconstructed water resources varied markedly from year to year. Mean discharge at Kudui Station was 18.07 m^3/s, and the period from 2005 to 2015 remained continuously low relative to the rest of the record. Mean annual water resources for 1978–2020 were 754 million m^3, of which 50%–70% occurred from July to September. Low-water years were also more common after 2000.

(3) Mean annual water resources are slightly lower in the future simulations than in the historical reconstruction, whereas interannual fluctuations become larger. The projected means are 652 million m^3 under SSP245 and 712 million m^3 under SSP585. The results therefore point to greater variability in future water availability rather than a large decline in its long-term mean.

REFERENCES

[1] Jia, Y., Wang, H., & Ni, G. (2005). Principles and practice of distributed watershed hydrological models. China Water & Power Press.

[2] Lu, M. (2021). Review and prospects of the Xinanjiang model. Journal of Hydraulic Engineering, 52(4), 432–441.

[3] Liu, J., & Zhang, W. (2018). Spatial variability in degree-day factors in Yarlung Zangbo River Basin in China. Journal of University of Chinese Academy of Sciences, 35(5), 704–711. https://doi.org/10.7523/j.issn.2095-6134.2018.05.018

[4] Martel, J. L., Demeester, K., Brissette, F., Poulin, A., & Arsenault, R. (2017). HMETS—A simple and efficient hydrology model for teaching hydrological modelling, flow forecasting and climate change impacts. International Journal of Engineering Education, 33(4), 1307–1316.

[5] Jia, Y., Wang, H., Qiu, Y., & Zhou, Z. (2006). Generalized water resources assessment based on the watershed water cycle model (I). Journal of Hydraulic Engineering, 37(9), 1051–1055.

[6] Liu, J., Zhou, Z., Jia, Y., Wang, H., & Chen, X. (2014). A stem–branch topological codification for watershed subdivision and identification to support distributed hydrological modelling at large river basins. Hydrological Processes, 28(14), 2074–2081. https://doi.org/10.1002/hyp.9746

[7] Xu, X., Liu, J., Zhang, S., Li, R., Yan, C., & Wu, S. (2018). China multi-period land use/cover remote sensing monitoring dataset (CNLUCC). Resource and Environmental Science Data Registration and Publishing System. https://doi.org/10.12078/2018070201

[8] Ye, Q. H., Zong, J. B., Tian, L. D., Cogley, J. G., Song, C. Q., & Guo, W. Q. (2017). Glacier changes on the Tibetan Plateau derived from Landsat imagery: Mid-1970s–2000–13. Journal of Glaciology, 63(238), 273–287. https://doi.org/10.1017/jog.2016.137

[9] Zhang, Y., Liu, S., & Wang, X. (2019). Spatial distribution dataset of degree-day factors for glaciers in High Mountain Asia. Science Data Bank. https://doi.org/10.11922/sciencedb.747

[10] Wang, K., Song, X., Lu, F., Yu, S., Zhou, Y., & Sun, J. (2024). CMIP6 simulation-based daily surface air temperature and precipitation projections over the Qinghai–Tibetan Plateau in the 21st century. Atmosphere, 15(4), 434. https://doi.org/10.3390/atmos15040434